ARCHIVES OF CIVIL AND MECHANICAL ENGINEERING

Vol. VIII 2008 No. 1

Computations of the propeller open water characteristics using the SOLAGA computer program. Predictions of the cavitation phenomenon

PAWEŁ DYMARSKI
Ship Design and Research Centre S.A. (CTO SA) – Ship Hydromechanics Division, 65, Szczecińska St., 80-392 Gdańsk

This paper presents the theoretical model and numerical methods which are applied in computer program SOLAGA for computations of viscous flow around ship propeller as well as for modelling of cavitation phenomenon. The model presented in the article is based on mass conservation equation and Reynolds averaged Navier-Stokes equation, the turbulent viscosity is approximated with the use of Spalart-Allmaras turbulent model. The numerical model used for solving the system of main equations is based on Finite Volume Method. The procedures for cavitation predictions applied in the SOLAGA program are based on travelling bubble model. This paper presents the results of computations of K_T, K_Q characteristics for conventional and skewed propeller. The results are compared with the data obtained from experiment. The results of computation of cavitation for the skewed propeller are presented as well.

Keywords: *propeller, viscous flow, CFD, cavitation, turbulence*

1. Introduction

The main target of the paper is to show state of development of computer program SOLAGA, especially its ability to solve problems connected with viscous flow around ship propeller with the use of periodic boundary conditions as well as to present the results of computations of cavitation. Program SOLAGA has been developed in the framework of research project supported by Polish Committee of Science. It has been also the main subject of the author's PhD thesis.

2. Governing Equations

The closed system of motion equations, derived for incompressible fluid, is based on the momentum and mass conservation laws. An integral form of mass conservation equation formulated for control volume Ω with a surface S reads

$$\int_S \rho \mathbf{v} \cdot \mathbf{n} \mathrm{d}S = 0, \tag{1}$$

and the conservation equation of i-th momentum component has the following form:

$$\frac{\partial}{\partial t}\int_{\Omega}\rho u_i \mathrm{d}\Omega + \int_{S}\rho u_i \mathbf{v}\cdot\mathbf{n}\mathrm{d}S = \int_{S}\left(\tau_{ij}\mathbf{i}_j - p\mathbf{i}_i\right)\cdot\mathbf{n}\mathrm{d}S\,, \tag{2}$$

where:

v is velocity vector,

u_i – i-th velocity component,

p – pressure,

ρ – density,

n – unit vector normal to S surface,

i_i – i-th component of Cartesian unit vector,

τ_{ij} is a viscous stress tensor.

When the flow is turbulent, **v** and u_i refer to mean velocity vector and mean i-th velocity component, p is a mean value of pressure. The word "mean" denotes average in a time period, which is long compared to the period of turbulent oscillations [5].

The viscous stress tensor τ_{ij} is specified by Boussinesq approximation [1], [5]:

$$\tau_{ij} = 2(\mu + \mu_t)S_{ij}, \tag{3}$$

where:

μ is a molecular viscosity,

μ_t is the turbulent viscosity,

S_{ij} is the mean strain-rate tensor.

The turbulent viscosity is calculated with the use of Spalart-Allmaras turbulence model [1], [5].

3. Cavitation

The cavitation model is based on travelling bubble method [4]. It is assumed in the model, that a large number of micro gas nuclei is present in the liquid. When pressure value decreases below a specified critical level, the radius of nucleus starts to grow rapidly and – according to the model – this is the inception of cavitation.

To determine behaviour of a single bubble the pressure field, velocity field (or bubble trajectory) and initial size of nucleus have to be given.

The single bubble dynamic is described by Rayleigh-Plasset equation:

$$R\frac{\mathrm{d}^2R}{\mathrm{d}t^2} + \frac{3}{2}\left(\frac{\mathrm{d}R}{\mathrm{d}t}\right)^2 + \frac{\mu}{\rho R}\frac{\mathrm{d}R}{\mathrm{d}t} = \frac{-p + \dfrac{2\mathrm{A}}{R} - p_v - p_g}{\rho}\,, \tag{4}$$

where:

R is a radius of the bubble,

t is time,

p is pressure far from the bubble,
p_v – vapour pressure,
p_g – pressure of the gas in the bubble,
A – denotes the surface tension coefficient.

When spectrum of nuclei at inflow is given (i.e. number of nuclei in a given range of radius) one can calculate nuclei distribution in every point inside the domain. Probability of cavitation phenomenon can be approximated by the following simplified formula:

$$P_{CAV} = \mathrm{cut}\left(\sum_i \frac{4}{3} \pi R_i^3 n_i \right), \tag{5}$$

where:

n_i is the number of nuclei of size R_i inside the unit volume and function cut(x) is defined as:

$$\mathrm{cut}(x) = \{x \text{ for } x \le 1; 1 \text{ for } x > 1\}. \tag{6}$$

4. Numerical Methods

The solution algorithm for solving the viscous flow is based on Finite Volume Method. The Finite Volume Method is based on integral form of conservation equations. The solution domain is subdivided into a finite number of control volumes, and the conservation equations are applied to each of them. The computational node at which the values of field functions are to be calculated lies at the centroid of each control volume (CV).

To express the value of each field quantity on CV surface S, suitable interpolation methods are used. In the presented program two methods are applied: upwind UDS (first order) and linear interpolation CDS (second order). Surface and volume integrals are approximated using midpoint quadrature [3]. As a result of FV discretization approach, one obtains an algebraic equation for each CV. The system of equations (after linearization) is solved using an iterative method. Two algorithms for solving the systems of algebraic equations are used: ICCG for symmetric systems and Bi-CGSTAB for non-symmetric systems [3].

When the problem of flow around a propeller is solved with the use of rotating grid, the problem becomes unsteady. The time integral in the Navier-Stokes equation is solved with the use of implicit Euler method.

a. Rotating grid

Computation of flow around ship propeller requires the use of rotating grid or rotating coordinate system. In the first method, the conservations equations have to be

modified in order to take into account a relative velocity between grid (control volumes) and coordinate system. The mass conservation of equation for single rotating control volume in integral form reads

$$\int_S \rho(\mathbf{v}-\mathbf{v}_b)\cdot\mathbf{n}\mathrm{d}S\,, \tag{7}$$

where:

$\mathbf{v}_b = \omega \times \mathbf{r}_b$ is a velocity of CV boundary,

ω – rotational velocity of the grid,

$\mathbf{r}_b$ – position vector of a point at S.

The momentum conservation equation for i-th momentum component takes the following form:

$$\frac{\mathrm{d}}{\mathrm{d}t}\int_\Omega \rho u_i \mathrm{d}\Omega + \int_S \rho u_i(\mathbf{v}-\mathbf{v}_b)\cdot\mathbf{n}\mathrm{d}S = \int_S \left(\tau_{ij}\mathbf{i}_j - p\mathbf{i}_i\right)\cdot\mathbf{n}\mathrm{d}S\,. \tag{8}$$

b. Periodic boundary conditions

In case of computation of open water characteristic of a propeller, it is possible to use periodic boundary conditions (Figure 1). This approach reduces the size of domain z – times (where z is a number of blades).

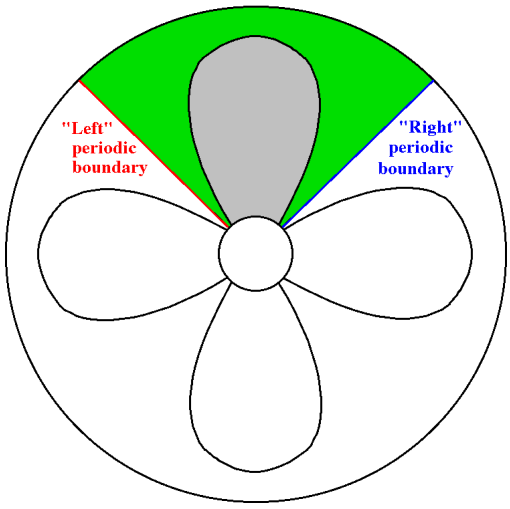

Fig. 1. Periodic subdomain and periodic “left” and “right” boundary conditions. The periodic subdomain covers only a single blade and its size is z times lower than size of whole domain. (z is a number of blades)

At the periodic boundaries we have the following conditions:

$$p_L = p_R, \qquad \varphi_L = \varphi_R, \qquad \mathbf{v}_L = \mathbf{Q}_{RL}\mathbf{v}_R, \tag{9}$$

where:
φ is a scalar quantity (i.e.: turbulent viscosity),
$\mathbf{Q}_{RL}$ is a transformation matrix from "right" R to "left" L periodic boundary:

$$\mathbf{Q}_{RL} = \begin{bmatrix} 1 & 0 & 0 \\ 0 & \cos\alpha & -\sin\alpha \\ 0 & \sin\alpha & \cos\alpha \end{bmatrix}, \tag{10}$$

$\alpha = 2\pi/z$ is an angle between left and right periodic boundary.

Non-matching interfaces

From the numerical point of view periodic boundary condition is an interface between two subdomains (Figure 2a, b). In SOLAGA solver, the grid at periodic interface may be non-matching, it allows to build almost orthogonal grids with better structure than "matching" meshes (Figure 2c, d).

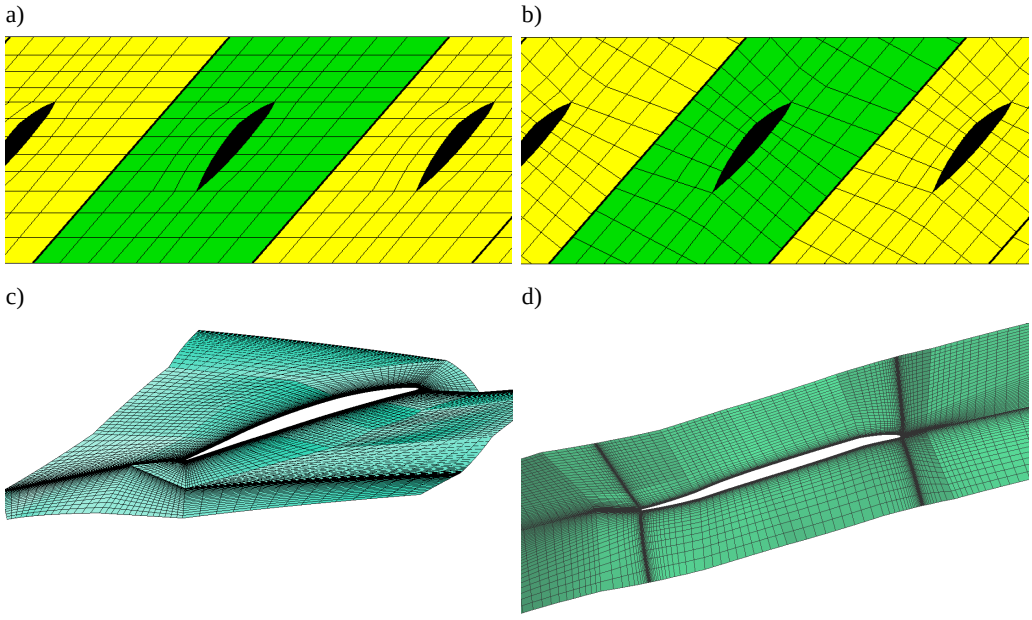

Fig. 2. Scheme of matching (a) and non-matching (b) connections at periodic boundary. Difference between structure of periodic matching (c) and non-matching grid (d) for calculation of flow around propeller blade

5. Computations

Computations were carried out for two propeller models: model A – conventional propeller and model B – skewed propeller. Computations were carried out with rotating grid and with the use of periodic boundary conditions with non-matching interfaces. The details of computational settings are presented in Table 1.

Table 1. Computational settings

Time step	0.0001 s
Number of iterations per time step	3
Interpolation scheme	CDS (blending factor 0.8)
Time integral approximation	Implicit Euler

a. Test case 1 – model A. Flow around conventional propeller

Geometry of the model A. Computational conditions

Table 2. Geometry of propeller model A

Type	Fixed pitch
No of blades	4
Diameter	183.90 mm
Pitch ratio at 0.7 radius	0.7413
Expanded area ratio	0.574
Hub ratio	0.175
Blade width at 0.7 radius	55.79 mm

Table 3. Open water test and computational conditions

	Test conditions	Computational conditions
Propeller revolutions n	28.0 1/s	28.0 1/s
Propeller velocity v_p	0.0–4.2 m/s	1.0; 2.0; 3.0; 4.0 m/s
Advance coefficient J	0.0–0.816	0.194; 0.388; 0.583; 0.777

The domain size and grid structure

Size of the domain: the inlet is located 2.3 D upstream from the propeller, the outlet is 2.2 D downstream, the diameter of the domain is 2.9 D. The boundary faces of the domain are presented in Figure 4a.

The grid was generated with the use of program ANSYS ICEM CFD Hexa. The grid is hexahedral and block-structured, number of CV's (per one blade) is 974 424. The grid structure on blade, hub and periodic surface is shown in Figure 4b.

Results of computations

Pressure distribution over the suction and pressure side of the propeller blade is presented in Figure 5.

a) b)

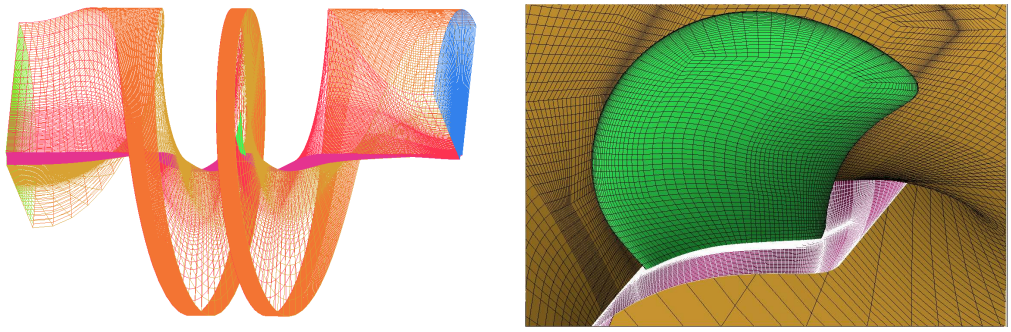

Fig. 4. a) Model A: domain of computations, b) Grid structure on the propeller blade, hub and periodic surface

The comparison of the calculated and experimental values of K_T and K_Q for several values of J is presented in Figure 6a.

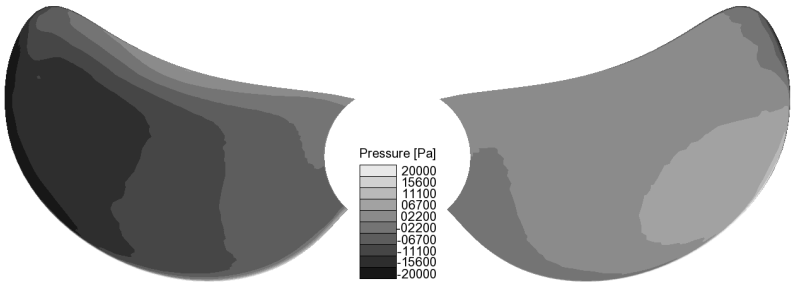

Fig. 5. Pressure distribution over the suction (left) and pressure (right) side of the conventional propeller, J = 0.388

a) b)

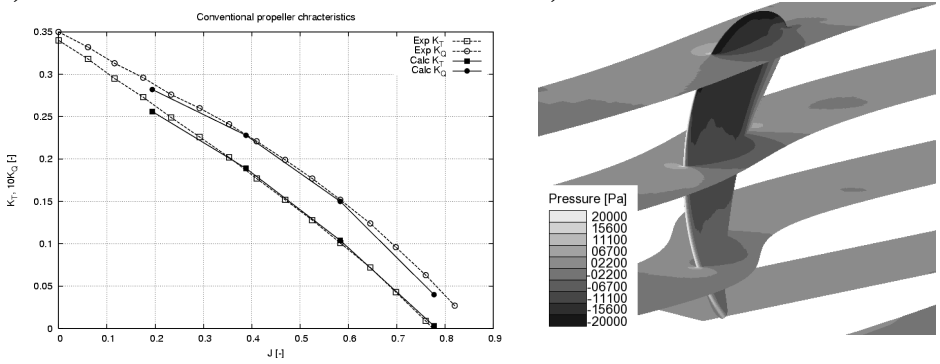

Fig. 6. a) K_T, K_Q characteristics of model A – conventional propeller, b) pressure distribution at the domain intersections, J = 0.388

b. Test case 2 - model B. Flow around skewed propeller

Geometry of the model B. Computational conditions

Table 4. Geometry of Propeller model B:

Type	Controllable pitch
No of blades	5
Diameter	265.73 mm
Pitch ratio at 0.7 radius	1.4281
Expanded area ratio	0.820
Hub ratio	0.3026

Table 5. Test and computational conditions:

	Test conditions:	Computational conditions:
Propeller revolutions n	11.0 1/s	11.0 1/s
Propeller velocity v_p	0.5–4.1 m/s	1.0; 2.0; 3.0; 4.0 m/s
Advance coefficient J	0.171–1.403	0.342; 0.684; 1.026; 1.368

Table 6. Data for computations of cavitation

Propeller velocity v_p	2.0 m/s
Advance coefficient J	0.684
Reference pressure (at inflow) p_0	0.04; 0.06; 0.08; 0.10 bar
Number of nuclei (at inflow) n_0	$0.1 \cdot 10^6$ 1/m^3
Radius of nuclei (at inflow) R_0	$10.0 \ 10^{-6}$ m

The domain size and grid structure

Size of the domain: the inlet is located 1.9 D upstream from the propeller, the outlet is 1.9 D downstream, the diameter of the domain is 2.4 D. The boundary faces of the domain are presented in Figure 7a.

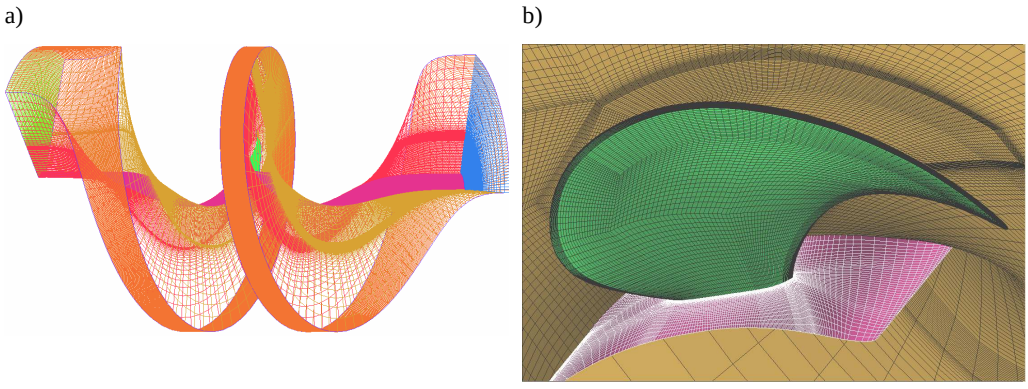

Fig. 7. a) Model B: domain of computations, b) grid structure on the propeller blade, hub and periodic surface

The grid was generated with the use of program ANSYS ICEM CFD Hexa. The grid is hexahedral and block-structured, number of CV's (per one blade) is 1 086 176. The grid structure on blade, hub and periodic surface is shown in Figure 7b.

Results of computations

Pressure distribution over the suction and pressure side of the propeller blade is shown in Figure 8. The comparison of the calculated and experimental values of K_T and K_Q for several J is presented in Figure 9a, however picture 9b shows pressure distribution inside the domain. The low pressure area which is stretched behind a blade tip is caused by a strong vorticity of tip vortex. The tip vortex is visible even far than 180 degrees behind the blade.

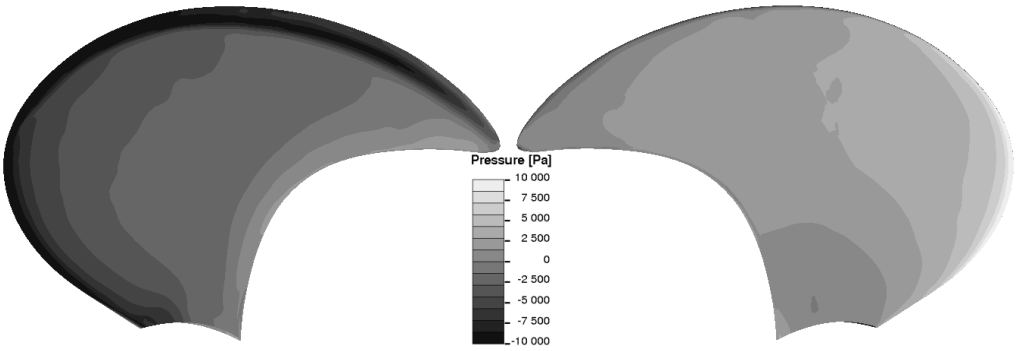

Fig. 8. Pressure distribution over a suction (left) and pressure (right) side of the skewed propeller, J = 0.684

a) b)

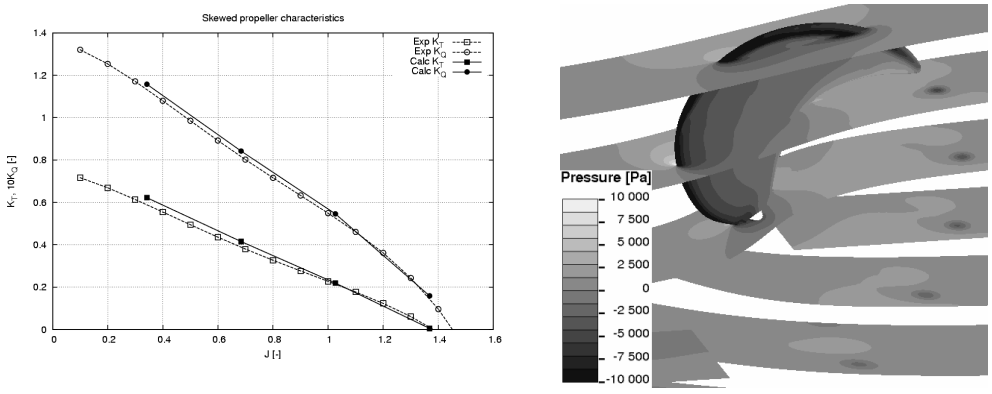

Fig. 9. a) K_T, K_Q characteristics of the skewed propeller (model B), b) pressure distribution at intersections of the domain, J = 0.684

Figure 10 presents distribution of probability of cavitation P_{CAV} at blade surface as well as the shape of isosurface $P_{CAV} = 0.5$ which can be treated as a face of large scale cavitation structures, e.g.: laminar cavitation, tip vortex cavitation or large bubbles. Bubble cavitation can be expected in regions where function of probability takes a value between about 0.1 and 0.5. The presented model does not predict secondary form of cavitation, e.g.: cloud cavitation.

Open water cavitation tests for the propeller are planned to be carried out in the near future. Up to now, the presented cavitation model has been validated on an example of hydrofoil [2].

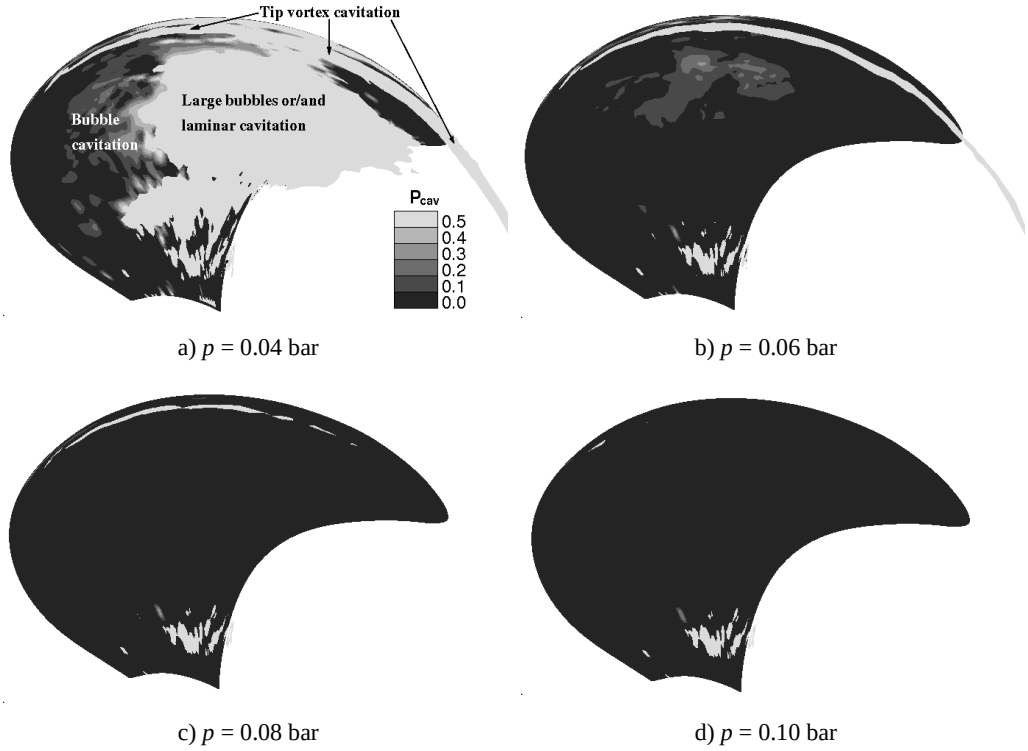

a) p = 0.04 bar b) p = 0.06 bar

c) p = 0.08 bar d) p = 0.10 bar

Fig. 10. Computational predictions of cavitation phenomenon on propeller blade for advance coefficient J = 0.684 and various values of reference pressure. The pictures shows probability of cavitation P_{CAV} on blade surface as well as isosurface $P_{CAV} = 0.5$

6. Conclusions

1. The calculated pressure distribution over the blades of the propellers is smooth, without any numerical oscillations, also there are no pressure oscillations near periodic, non-matching boundaries.

2. The calculated propeller characteristics: thrust K_T, and torque K_Q coefficients are in good agreement with the experimental results for both conventional and skewed propeller.

3. Program SOLAGA can be also a good tool for the tip vortex modelling. The low pressure area caused by vorticity is clearly visible far behind the propeller blade (Figure 9 b). Close examination of his figure shows the core of the vortex created by the next blade.

4. Figure 10, in which the probability of cavitation is presented, shows the structures of cavitation like those observed on similar propeller models in cavitation tunnel. One can distinguish the elongated structure of tip vortex cavitation which spreads from leading edge, through the tip, to the slipstream (Figure 10a–10c). The regions are also visible where bubble cavitation may appear, where P_{CAV} ranges from about 0.1 to 0.5 (Figure 10a, b) as well as large area where laminar or/and developed bubble cavitation can be expected (Figure 10a).

References

[1] Blazek J.: *Computational Fluid Dynamics: Principles and Applications*, ELSEVIER 2001.
[2] Dymarski P.: *Numerical computation of hydrodynamic forces on hydrofoil. Prediction of cavitation phenomenon*, 8th Numerical Towing Tank Symposium, 2–4 Oct., 2005, Varna.
[3] Ferziger J.H, Peric M.: *Computational Methods for Fluid Dynamics*, 2nd ed., Berlin, Springer, 1999.
[4] Lecoffre Y.: *Cavitation. Bubble Trackers*, A. A. Balkema/Rotterdam/Brookfield, 1999.
[5] Wilcox D.C.: *Turbulence Modeling for CFD*, DCW Industries, 2002.

Obliczenia charakterystyk śrub swobodnych przy użyciu programu komputerowego SOLAGA. Prognozowanie zjawiska kawitacji

Niniejszy referat prezentuje pokrótce model teoretyczny oraz metody obliczeniowe zastosowane w programie komputerowym SOLAGA służącym do obliczeń opływu lepkiego śruby okrętowej oraz do wykonywania obliczeniowych prognoz występowania zjawiska kawitacji. W pracy zastosowano model cieczy lepkiej oparty na równaniu zachowania masy oraz równaniu zachowania pędu (rów. Naviera-Stokesa) w formie uśrednionej Reynoldsa. Lepkość turbulentna aproksymowana jest przy użyciu modelu turbulencji Spalarta-Allmarasa. Model numeryczny zastosowany do rozwiązania głównego układu równań bazuje na metodzie objętości skończonej. Metodę prognozowania zjawiska kawitacji oparto na modelu unoszonego pęcherzyka. W artykule przedstawiono ponadto wyniki obliczeń w formie rozkładu ciśnień oraz charakterystyk K_T, K_Q śruby, które zostały porównane z danymi doświadczalnymi. Przedstawione zostały również wyniki obliczeń kawitacji na skrzydle śruby okrętowej.